Molecular Dynamics Simulations of Supported Pt Nanoclusters with Sutton-Chen Potentials

Jeffrey M. Moore
Department of Physics, University of Washington, Seattle, WA 98195
(Dated: September 26, 2013)

Understanding the physical and chemical behavior of supported nanoscale catalysts is of fundamental and technological importance. However, much of nanocatalyst behavior remains poorly understood due to the complex, dynamical nature of catalytic interactions at a nanomolecular scale. It has been demonstrated that real-time ab-initio calculations may provide fundamental insight into the dynamical electronic and physical structure of catalytic nanoparticles, yet these calculations can prove to be extremely computationally intensive. In order to examine longer time relaxations of these systems, we have used a classical molecular dynamics simulation based on the Sutton-Chen potential to model Pt_{10} nanoparticles supported on a [110] γ-Al_2O_3 surface. Results are compared to previous density functional theory/molecular dynamics (DFT/MD) simulations, and calculated thermal and diffusive properties are presented.

INTRODUCTION

Nanoparticles are very attractive candidates as catalysts due to an increased surface to volume ratio compared to bulk materials, allowing for increased selectivity for chemical reactions.[1] Nanocatalysis is widely used over a range of industrial applications, including catalytic conversion of vehicle emissions and petroleum reformation.[2] However, despite being one of the oldest applications of nanoscience,[1] the mechanism of nanocatalysis is not very well understood due to the complex, dynamical nature of catalytic interactions at a nanomolecular scale. Previous x-ray absorption spectroscopy (XAS) experiments have reported that oxide-supported Pt_{10} nanoparticles display a variety of interesting characteristics, such as large structural disorder, negative thermal expansion, and thermally induced changes in electronic structure.[3] Density Functional Theory/Molecular Dynamics (DFT/MD) calculations have been implemented previously to investigate these systems, and have successfully reproduced many of the phenomena described in these XAS experiments. Given that nanocatalysis presents a chemically complex system in which surface reactions give rise to many different interatomic interactions and the electronic structure of the system is changing qualitatively with time, ab-initio molecular dynamics calculations are well-suited in exploring the dynamic nature of these systems.[4]

Nevertheless, DFT/MD calculations can prove to be impractical in terms of sheer computational demand. When restricted to ab-intio calculations, the phase space accessibility of a system becomes largely dependent on the affordability of computational resources. Previous DFT/MD calculations of Pt_{10} nanoclusters have required more than 10^4 cpu hours of computation for systems with time evolutions ranging near 10 picoseconds.[5] Thus, physical quantities requiring long relaxation times, such as diffusive properties and long-period thermal fluctuations, are tremendously difficult to resolve using ab-initio methods.

The purpose of our classical molecular dynamics simulation is to offer an economical alternative to ab-initio molecular dynamics in terms of computational tractability. Our approach utilizes a potential model introduced by Sutton and Chen which employs many-body terms.[6] The potential is tailored for f.c.c. transition metals and has been shown to accurately model long range van der Waals pair interactions and approximate the many-body metallic bonding of the crystal.[7] The Sutton-Chen potential has been successfully applied in many other studies and has demonstrated a reasonable agreement with experiment.[8] More importantly for the purposes of our model, the potential can be implemented in simulation without necessarily requiring the calculations to be computationally intensive. The speed of our calculations allows us to probe very long time evolutions of many different nanoscale systems. Furthermore, the parameterized form of the potential provides a flexibility for the model, allowing the potential to be readily adjusted as needed dependent on an individual system, although such methods are not addressed in the scope of this paper. The results of previous DFT/MD calculations will be compared to those of the potential model, when possible, using unadjusted parameters for Pt provided by Sutton and Chen. In addition, energy fluctuations, autocorrelation functions, and the temperature-dependent diffusivity of the Pt_{10} nanoparticles are presented.

MODEL POTENTIALS

Three different potentials are used to model the dynamics of the simulation in order to most accurately represent the interactions between the nanocluster and substrate. The intracluster interactions are modeled using the Sutton-Chen potential as noted in the introduction. The Sutton-Chen potential is a Finnis-Sinclair type potential with two terms providing the pair-wise repulsive

TABLE I: Model potential parameters used in the simulation.

Potential	ϵ (eV)	σ (Å)	a (Å)	c	n	m
$U_{SC,Pt-Pt}$	1.9835×10^{-2}		3.92	34.408	10	8
$U_{LJ,Pt-O}$	0.228	1.866				
$U_{LJ,Pt-Al}$	0.044	2.420				

and approximate many-body cohesive contributions separately. The form of the potential is:

$$U_{SC} = \epsilon \sum_i \left(\frac{1}{2} \sum_{j \neq i} V_{r_{ij}} - c\sqrt{\rho_i} \right) \tag{1}$$

$$V_{r_{ij}} = \left(\frac{a}{r_{ij}} \right)^n \tag{2}$$

$$\rho_i = \sum_{j \neq i} \left(\frac{a}{r_{ij}} \right)^m \tag{3}$$

where the $V_{r_{ij}}$ and $\sqrt{\rho_i}$ terms serve as the repulsive and many-body contributions, respectively. The parameters of the potential are defined by Sutton and Chen for a variety of transition metals.[7] ϵ is a scaling term with dimensions of energy, a is the lattice constant, c is a dimensionless constant, and n and m are positive integers such that $n > m$. The parameters for Pt are listed in Table I.

The substrate of the system is modeled by atoms which oscillate in three dimensions about fixed points in space, corresponding to a [110] Al_2O_3 surface, according to a harmonic potential:

$$U_H = \frac{1}{2} k r_e^2 \tag{4}$$

where r_e is the displacement of the surface atom from its equilibrium position. The restoring parameter k is chosen to be 6.0 eV/Å^2, such that the oscillation frequency and mean square displacement of the oxygen atoms correspond to experimental values.[3] The interaction between the Pt_{10} cluster and the Al_2O_3 surface is modeled separately using a Lennard-Jones potential, given by:

$$U_{LJ} = 4\epsilon \left(\left(\frac{\sigma}{r_{ij}} \right)^{12} - \left(\frac{\sigma}{r_{ij}} \right)^{6} \right) \tag{5}$$

The Pt-O and Pt-Al interactions each use separate potential parameters ϵ and σ. The parameters were determined by adjusting the parametric equation of the radial distribution function for Lennard-Jones fluids to reproduce the same distributions for Pt-O and Pt-Al interactions produced by ab-initio molecular dynamics simulations. The parameters are also listed in Table I. The cluster forces $\boldsymbol{F}_C$ and surface forces $\boldsymbol{F}_S$ are then given by the gradient of their respective potentials.

$$\boldsymbol{F}_C = -\boldsymbol{\nabla} \left(U_{SC} + U_{LJ} \right) \tag{6}$$

$$\boldsymbol{F}_S = -\boldsymbol{\nabla} \left(U_H + U_{LJ} \right) \tag{7}$$

COMPUTATIONAL DETAILS

Algorithms

The simulation uses the velocity-Verlet algorithm with the Nosé-Hoover thermostat to evolve the system in time at constant temperature. The velocity-Verlet algorithm is a well known second-order symplectic integration scheme for solving the canonical equations of motion, and is well-regarded for its accuracy in preserving the phase space behavior of its system.[9–11] The Nosé-Hoover thermostat algorithm, like velocity-Verlet integration, is also used extensively by the molecular dynamics community for being a deterministic, stable, and time-reversible method of simulating constant-temperature dynamics.[12] Incorporating the Nosé-Hoover with the velocity-Verlet scheme, the algorithm to evolve the system from a time t to a short time later $t + h$ is given by the following equations:

$$\boldsymbol{r}(t+h) = \boldsymbol{r}(t) + h\boldsymbol{v}(t) + \frac{h^2}{2}\left(\frac{\boldsymbol{F}(t)}{m} - \zeta(t)\boldsymbol{v}(t) \right) \tag{8}$$

$$\boldsymbol{v}(t+\frac{h}{2}) = \boldsymbol{v}(t) + \frac{h}{2}\left(\frac{\boldsymbol{F}(t)}{m} - \zeta(t)\boldsymbol{v}(t) \right) \tag{9}$$

$$\zeta(t+h) = \zeta(t)\frac{h}{2Q}\left(K(t) + K(t+\frac{h}{2}) - 2Nk_BT_0 \right) \tag{10}$$

$$\boldsymbol{v}(t+h) = \frac{2}{2+h\zeta(t+h)} \cdot \left(\boldsymbol{v}(t+\frac{h}{2}) + \frac{h}{2}\frac{\boldsymbol{F}(t+h)}{m} \right) \tag{11}$$

$K(t)$ is the kinetic energy of the system at time t, T_0 is the thermostat temperature, N is total number of degrees of

freedom of the system, and k_B is the Boltzmann constant. The ζ term is a variable derived from the addition of a virtual degree of freedom into the Hamiltonian, which dictates the effective temperature relaxation time.[12] ζ incorporates an analogous thermal inertia quantified by "mass" Q, and both are given by:

$$\zeta(t) = \frac{2K(t) - Nk_BT_0}{Q} \tag{12}$$

$$Q = N_{DoF}k_BT_0\tau^2 \tag{13}$$

where τ is the characteristic time describing the strength of the coupling to the heat bath. τ cannot be chosen arbitrarily, but must be selected such that the Nosé-Hoover thermostat remains thermally coupled to the system. Loose coupling will lead to poor temperature control, while tight coupling results in high frequency oscillations in the temperature. For the purposes of our simulation, τ is chosen to be 0.2 ps.

Simulation Conditions

Simulations were carried out using a Pt_{10} nanocluster on a [110] surface of γ-Al_2O_3 over a range of temperatures between 100 K and 800 K. Simulation times of 210 ps and 1.01 ns were run with temperature separations of 25K and 100 K respectively. Initial configurations of the cluster were selected from a trajectory of a thermalized Pt_{10} nanocluster in free space at a random time, to ensure an initial potential near a local minima. The cluster is placed in close proximity to the γ-Al_2O_3 surface and allowed 10 ps to adsorb and thermalize before the remaining trajectory is used for resulting calculations. Multiple initial configurations were used at each temperature. Initial velocities of the atoms were randomized with a normal distribution and rescaled to produce energies corresponding to the system thermostat.

RESULTS AND DISCUSSION

Internal Structure and Dynamics

The internal structure of the Pt_{10} nanocluster can be characterized by the pair distribution function (PDF) $g(R)$, which indicates the relative probability of finding a pair of atoms within the cluster with separation R_{Pt-Pt}. A plot of $g(R)$ for Pt_{10} for a number of temperatures is shown in FIG. 1. At lower temperatures, $g(R)$ exhibits very structured second and third Pt-Pt coordination shells which diminish with increasing temperature. These results differ from those of previous ab-initio calculations which do not display any well-ordered structure beyond the first coordination shell. This is likely due to the long range attractive term of the Sutton-Chen potential, which may lead to an over-structured behavior of the cluster. Furthermore, the distributions of the first atomic coordination shells of the PDFs are not as sharply peaked as those seen in DFT/MD, as will be discussed further below. Visual inspection of the system reveals dynamic bond breaking and reforming between the nanocluster and surface with large librational motion between surface-bonded and non-surface-bonded atoms. The cluster experiences sizeable center of mass fluctuations which scale with increasing temperature, resulting in translation across the surface at high temperatures.

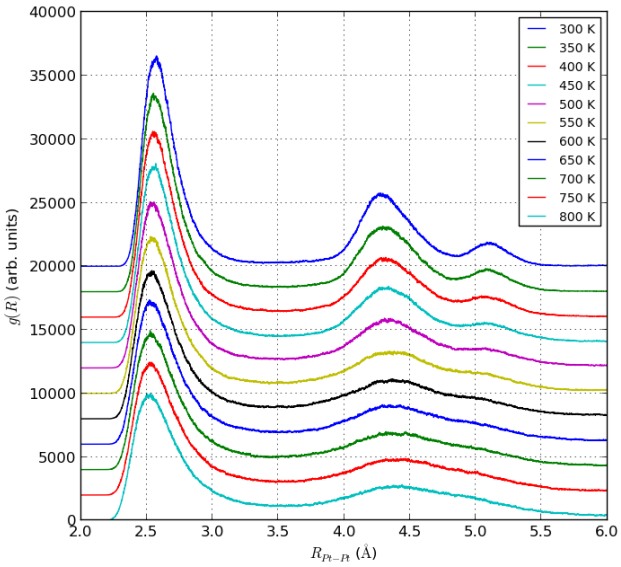

FIG. 1: Averaged pair distribution function (PDF) for a Pt_{10} cluster at various temperatures. The PDFs are averaged over 10 trajectories each with randomized initial cluster configurations. At low temperatures, the PDFs exhibit structured second and third Pt-Pt coordination shells. The attenuation of these shells with increasing temperature is indicative of the melting of the structure.

Another important physical quantity is the Debye-Waller factor (DWF), which describes the attenuation of x-ray scattering due to the thermal motion of atoms within a crystal. In this case, the DWF is indicative of the thermally-induced vibrational disorder of the cluster, and is proportional to the mean square relative displacement (MSRD) between Pt-Pt pairs. A Gaussian fit of the first coordination shell (FIG. 2), determined by enforcing a cut-off of 3.2 Å on the PDF, was used to determine the mean distances and MSRDs of atomic pairs, μ and σ^2 respectively. FIG. 3 gives an indication of how μ, σ^2, and mean coordination numbers vary with temperature. As mentioned before, the distributions of the first coordination shell are more broad than those found by DFT/MD. Values of σ^2 obtained by DFT/MD for Pt_{10}

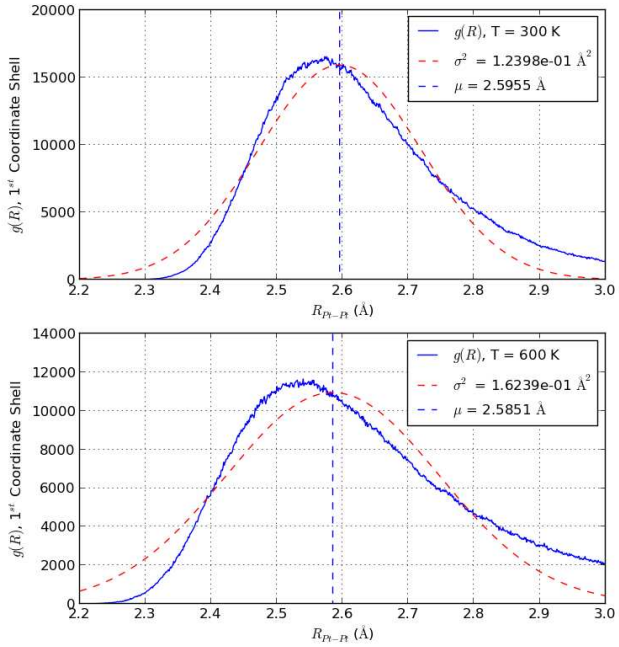

FIG. 2: Averaged 1st shell pair distribution function with Gaussian fit for temperatures of 300 K and 600 K. The doubling of σ^2 corresponds to a doubling of the temperature as expected, and an average decrease in mean atomic distance can be seen from the plots of μ.

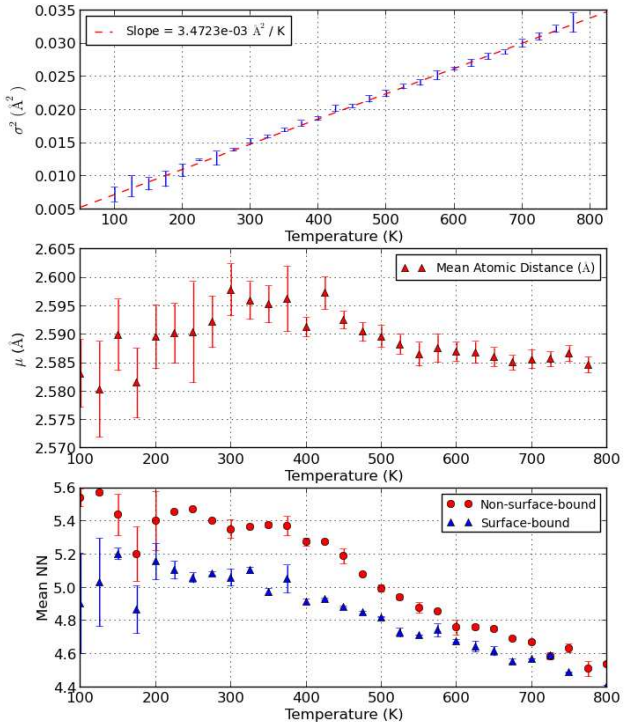

FIG. 3: Three temperature-dependent plots characterizing the intracluster dynamics of Pt_{10}. At the top is a plot of σ^2 which corresponds to the Debye-Waller factors, and depicts a linear increase of thermal disorder with an increase of temperature. At the center are the mean distances between Pt-Pt pairs which exhibit a decreasing trend at higher temperatures. The bottom plot relates the mean first coordination number with the temperature of the system. The results were averaged over the results of 10 unique initial conditions for each temperature, and the error bars correspond to their standard deviation.

were 5.2×10^{-3} Å^2 and 10.0×10^{-3} Å^2 for temperatures of 165K and 573K respectively, which are smaller than the values obtained by the MD simulation by about a factor of two.[5] The mean distances μ are in rough agreement with DFT/MD as well as experimental values (within 0.01 Å) and exhibits a decrease with higher temperatures suggestive of negative thermal expansion. However, a decrease of μ is not seen between temperatures of 175K and 575K as observed in x-ray absorption spectroscopy experiments.[3] The mean first neighbor coordination numbers found by the simulation are in much better agreement with the experimental value (~ 5.5) for 5-25 atom clusters when compared to DFT/MD calculations which give a mean of ~ 3 nearest neighbors for Pt_{10}.[5]

Thermal Properties

The thermal properties of the Pt_{10} nanocluster will differ considerably from those of bulk materials due to finite size effects. A substantial discussion of the thermal properties of nanoscale systems is provided elsewhere.[13] To summarize, the energy of the cluster is not well-defined, but instead characterized by energy fluctuations between the cluster and the surface. Energy fluctuates between the two with a probability distribution given by:

$$P(E,T) \approx \Omega(E)e^{-\beta E} = e^{-\beta \mathcal{F}(E,T)} \qquad (14)$$

where $\Omega(E)$ is defined as the number of microstates available to the system at energy E with $k\ln(\Omega(E)) = S(E)$ and $\mathcal{F}(E,T) = E - TS(E)$. Assuming equipartition, the mean energy will be $\langle E\rangle = 3NkT$ and the entropy will be given by $S(E) \approx 3Nk\ln(E/E_0)$. Since the probability distribution is approximately Gaussian, we can find the fluctuations about the mean energy $\langle E\rangle$ by taking the second derivative of the entropy, $\sigma_E^2 = k/\left(\partial^2 S(E)/\partial E^2\right)$. The energy fluctuations are then expected to be $\sigma_E = \langle E\rangle/\sqrt{3N}$.[13] The kinetic energy probability distribution of the system at 300 K and 600 K is shown in FIG. 4 along with the predictions of the the-

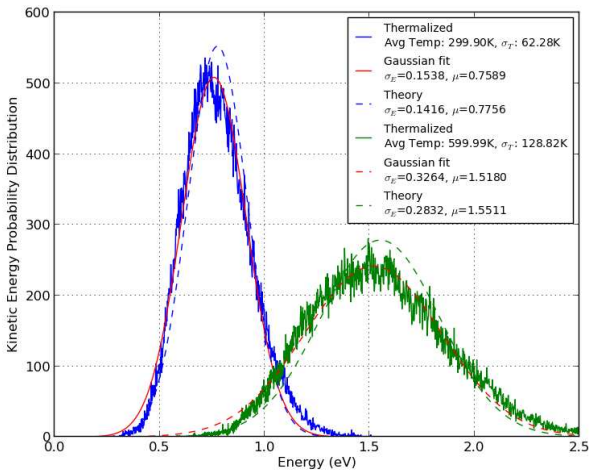

FIG. 4: Kinetic energy probability distributions for systems at temperatures of 300 K and 600 K fitted to a Gaussian distribution. The mean energies and fluctuations are compared to those predicted by the theory, $\langle E\rangle = 3NkT$ and $\sigma_E = \langle E\rangle/\sqrt{3N}$. The Nosé-Hoover equations produce mean energies within 2.6% of $\langle E\rangle$, and the relative fluctuations are greater by 8.6% and 15.2% for temperatures of 300 K and 600 K respectively.

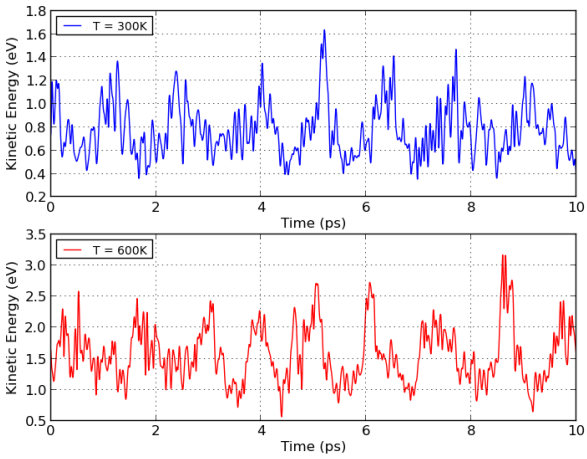

FIG. 5: Kinetic energy fluctuations with respect to time for systems with temperatures of 300 K and 600 K. The near-periodicity of the fluctuations is due to the oscillatory flow of heat between the Pt_{10} nanocluster and the γ-Al_2O_3 surface. The thermal energy of the surface is held at a constant, and serves as a heat bath for the Nosé-Hoover thermostat.

ory. The simulation energies are found to be within 2.6% of the expected value, and the fluctuation discrepancies scale with the temperature, with differences of 8.6% and 15.2% for temperatures of 300 K and 600 K respectively.

As noted previously, the Nosé-Hoover equations used in the simulation result from a virtual variable introduced into the Hamiltonian, resulting in the temperature dampening term ζ, described by Eqn. 12. Due to the nature of ζ, heat is allowed to flow between the heat bath and the system, regulating the system temperature. Heat flowing in or out of the system will do so in an oscillatory manner, which results in approximately periodic fluctuations in temperature about the thermal equilibrium value.[12] The frequency of these oscillations is driven by the "thermal inertia" Q, given by Eqn. 13, which determines the coupling of the thermostat. If coupled properly, the Nosé-Hoover thermostat will produce thermal fluctuations on order of σ_E, as shown in FIG. 4. These near-periodic oscillations can be seen in FIG. 5.

Diffusive Properties

The mass-transport processes of the Pt nanocluster are good indicators of its performance as a catalyst, which will depend upon the structural properties and accessibility of the nanoparticle. The Green-Kubo method of calculating the self-diffusion coefficient relies on the velocity autocorrelation function (VACF) of the system,[14] and is given by:

$$D = \frac{1}{3}\int_{t=0}^{\infty}\left(\frac{1}{N}\sum_{i}^{N} v_i(0)\cdot v_i(t)\right)dt \qquad (15)$$

While it is necessary to make this an infinite integral in theory, in practice the VACF is averaged over many intervals within a single MD trajectory to allow for smaller statistical errors.[15] The VACF is a measurement of the rate at which the system velocities no longer correspond to their initial values, or rather, how quickly the system loses the information of its initial conditions. The VACF of the system at three different temperatures can be seen in FIG. 6, with higher temperatures corresponding to a more rapid degradation of the "memory" of the system.

The self-diffusion coefficients D were determined using both the 210 ps and 1010 ps MD trajectories and are plotted in FIG. 7. The longer trajectories provide superior averaging of the VACF, increasing the accuracy of the results and allowing the 210 ps diffusion coefficients to be cross-referenced. The trend of D with temperature masks two different power-laws, corresponding to two possible regimes of reactivity.[16] If we assume the reaction rate of the system obeys an Arrhenius equation, the diffusion coefficients can be used to give activation energies for the different diffusive processes of Pt_{10} nanoclusters, corresponding to the slope of their linear fit on an Arrhenius plot as seen in FIG. 7.[16] At least two regimes of reactivity are clear in the plot, with one activation barrier appearing in the range of 300 K to 400 K. Interestingly, both the plots of mean distances and

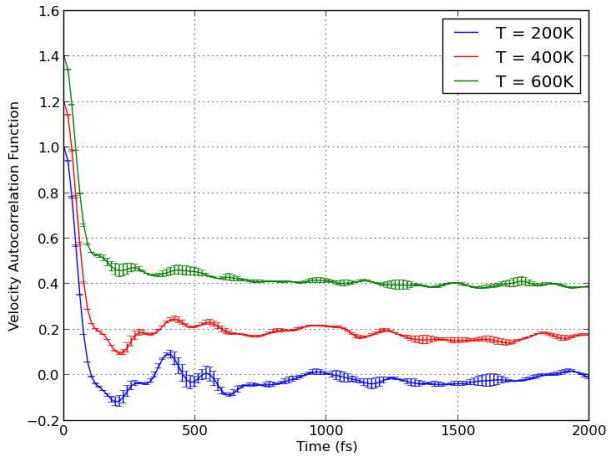

FIG. 6: Velocity autocorrelation function for three different temperatures, 200 K, 400 K, and 600 K. The attenuation of the curve corresponds to a degrading "memory" of the initial velocities of the system. Predictably, higher temperatures increase the rate of the degradation. The VACFs were averaged over 10 unique initial conditions at each temperature, and the error bars correspond to the standard deviation of their results.

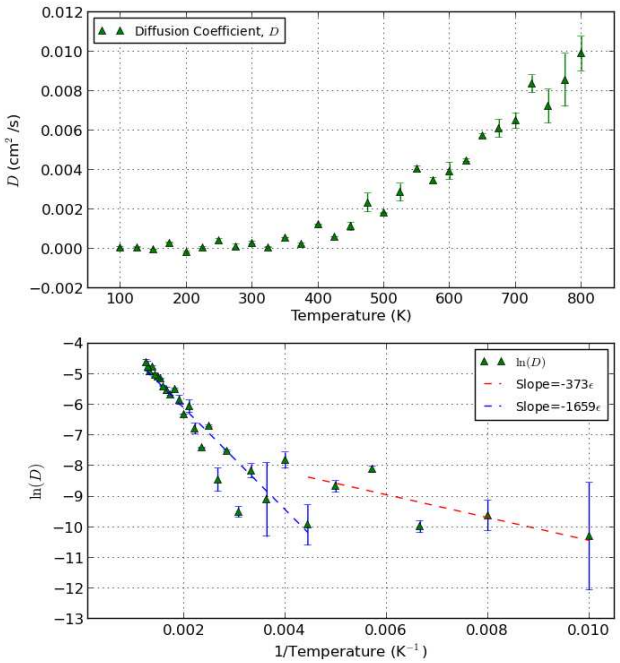

FIG. 7: Plots of the diffusion coefficients, D. In the first plot, D are plotted for various temperatures. The second Arrhenius plot shows the different regimes corresponding to different diffusion processes and activation energies given by D. The slope has units of negative temperature.

nearest neighbors seem to corroborate the existence of a regime change in the proximity of 400K; while the self-diffusion coefficient begins to rise rapidly with increasing temperature beyond 400K, the mean first atomic coordination number begins to fall and the mean distances between Pt-Pt pairs decrease. This may be an indication of a phase transition of the Pt_{10} nanoparticle.

SUMMARY

We have presented a method of calculating the dynamical properties of nanoscale systems with classical molecular dynamics simulations utilizing a model potential. The Sutton-Chen potential is used with unadjusted potential parameters for Pt provided by Sutton and Chen. The simulation is capable of probing very long time relaxations at low computational expense, allowing for calculation redundancy in exchange for increased statistical accuracy of the final results. The Nosé-Hoover thermostat equations are used with the velocity-Verlet algorithm and reproduce the referenced theoretical model for nanoscale thermodynamics, indicating that the equations sample a canonical ensemble.[12] The simulation provides trajectories with time scales necessary to arrive at possible values for self-diffusion coefficients, which have been calculated for temperatures in the range of 100 K to 800 K. The coefficients suggest that there are at least two regimes of temperature-dependent diffusivity processes, with an activation barrier near 400 K. The structural properties of Pt_{10} nanoclusters have been compared between the the results of the classical MD simulation and previous ab-initio MD calculations. Pair distribution functions produced by the Sutton-Chen potential are found to be over-structured compared to DFT/MD; the second and third atomic coordination shells are pronounced at lower temperatures, and the first atomic coordination shell is more broad, corresponding to Debye-Waller factors that are greater than those found in DFT/MD by about a factor of two. Nevertheless, the flexibility of the potential model enables the potential parameters to be adjusted if necessary to arrive at results that are consistent with ab-initio calculations and experiment. With adjusted parameters, the simulation could prove to be a powerful analytical tool for the investigation of long-time relaxations in dynamic nanoscale systems.

ACKNOWLEDGEMENTS

The author would like to thank advisors John J. Rehr and Fernando D. Vila for their outstanding support and mentorship. The author is also grateful to REU program directors Subhadeep Gupta and Alejandro Garcia as well

as the rest of the staff at the Institute of Nuclear Theory for facilitating the research. Financial support was provided by the National Science Foundation.

[1] Robert Schlgl and Sharifah Bee Abd Hamid. Nanocatalysis: Mature science revisited or something really new? *Angewandte Chemie International Edition*, 43(13):1628–1637, 2004.

[2] G.J. Antos and A.M. Aitani. *Catalytic Naphtha Reforming*. Chemical Industries Series. Marcel Dekker Incorporated, 2004.

[3] J. H. Kang, L. D. Menard, R. G. Nuzzo, and A. I. Frenkel. Unusual non-bulk properties in nanoscale materials: Thermal metal-metal bond contraction of g-alumina-supported pt catalysts. *J. Am. Chem. Soc.*, 128:12068, 2006.

[4] D. Marx and J. Hutter. Ab initio molecular dynamics: Theory and implementation. In J. Grotendorst, editor, *Modern Methods and Algorithms of Quantum Chemistry*, pages 301–449. Forschungszentrum Jlich, 2000.

[5] F. Vila, J. J. Rehr, J. Kas, R. G. Nuzzo, and A. I. Frenkel. Dynamic structure in supported pt nanoclusters: Real-time density functional theory and x-ray spectroscopy simulations. *Phys. Rev. B*, 78:121404, Sep 2008.

[6] A. P. Sutton and J. Chen. Long-range finnissinclair potentials. *Philosophical Magazine Letters*, 61(3):139–146, 1990.

[7] H. Rafii-Tabar and A. P. Sutton. Long-range finnis-sinclair potentials for f.c.c. metallic alloys. *Philosophical Magazine Letters*, 63(4):217–224, 1991.

[8] Jonathan P. K. Doye and David J. Wales. Global minima for transition metal clusters described by sutton-chen potentials. *New J. Chem.*, 22:733–744, 1998.

[9] Glenn J. Martyna, Douglas J. Tobias, and Michael L. Klein. Constant pressure molecular dynamics algorithms. *The Journal of Chemical Physics*, 101(5):4177–4189, 1994.

[10] Loup Verlet. Computer "experiments" on classical fluids. i. thermodynamical properties of lennard-jones molecules. *Phys. Rev.*, 159:98–103, Jul 1967.

[11] Ronald D. Ruth. A canonical integration technique. *Nuclear Science, IEEE Transactions on*, 30(4):2669–2671, 1983.

[12] Philippe H. Hunenberger. Thermostat algorithms for molecular dynamics simulations. In Christian Holm and Kurt Kremer, editors, *Advanced Computer Simulation*, volume 173 of *Advances in Polymer Science*, pages 105–149. Springer Berlin Heidelberg, 2005.

[13] J. J. Rehr and F. D. Vila. Shake-rattle-and-roll: A model of dynamic structural disorder in supported nanoscale catalysts, 2013.

[14] G.A. Fernndez, J. Vrabec, and H. Hasse. Self diffusion and binary maxwellstefan diffusion in simple fluids with the greenkubo method. *International Journal of Thermophysics*, 25(1):175–186, 2004.

[15] William H. Press, Saul A. Teukolsky, William T. Vetterling, and Brian P. Flannery. *Numerical Recipes 3rd Edition: The Art of Scientific Computing*. Cambridge University Press, New York, NY, USA, 3 edition, 2007.

[16] Arthur F. Voter. Classically exact overlayer dynamics: Diffusion of rhodium clusters on rh(100). *Phys. Rev. B*, 34:6819–6829, Nov 1986.